Cavity-Induced Optical Nonreciprocity Based on Degenerate Two-Level Atoms

Chuanzhao Qi , Jiarui Zheng , Yuanhang Tong , Ruonan Li , Dan Wang , Lianghui Huang , Haitao Zhou *

Posted Date: 18 June 2024

doi: 10.20944/preprints202406.1244.v1

Keywords: optical nonreciprocity; single dark-state peak; degenerate two-level; strong-coupling

Article

Cavity-Induced Optical Nonreciprocity Based on Degenerate Two-Level Atoms

Chuan-Zhao Qi [1], Jia-Rui Zheng [1], Yuan-Hang Tong [1], Ruo-Nan Li [2], Dan Wang [2,3], Liang-Hui Huang [2,3] and Hai-Tao Zhou [1,2,3]*

[1] Sanli Honors College, Shanxi University, Taiyuan, 030006, China
[2] State Key Laboratory of Quantum Optics and Quantum Optics Devices, Institute of Opto-Electronics, School of Physics and Electronic Engineering, Shanxi University, Taiyuan, 030006, China
[3] Collaborative Innovation Center of Extreme Optics, Shanxi University, Taiyuan, 030006, China
* zht007@sxu.edu.cn

Abstract: We propose and experimentally realize a scheme of the optical nonreciprocity (ONR) using degenerate two-level atoms embedded in an optical ring cavity. For the degenerate transition F_g=4→F_e=3, we first study the cavity-transmission property in different coupling field, and verify that within the strong-coupling regime, the single-dark-state peak formed by electromagnetically induced transparency (EIT) shows ONR. Qualitative theoretical analysis shows that the stable ground-state Zeeman coherence is necessary for intracavity EIT. However, due to the frequency degeneracy, the large Rabi frequency of counter-propagating coupling field can reduce the number of effective atoms and weaken the strong-coupling of the atom-cavity, which determines that ONR based on intracavity EIT occurs only at weaker probe intensity. Furthermore, the ONR transmission with high contrast, linewidth-narrowed and broadband is experimentally demonstrated.

Keywords: optical nonreciprocity; single dark-state peak; degenerate two-level; strong-coupling

1. Introduction

Optical nonreciprocity (ONR) has attracted widespread interest due to its important applications in optical communications and optical information processing [1–3]. Traditionally, ONR has been achieved through the magneto-optical effect [4], which poses challenges in miniaturization and integration. Thus, the exploration of magnet-free ONR avenues has emerged in recent years. Significant advancements have been made using methods such as nonlinear optics [5–7], optomechanical interactions [8–10], chiral quantum optics [11–13], tunable photonic crystals [14,15], cold atomic Bragg lattices [16,17], and hot atoms [18–22].

One of the important methods to realize ONR is the utilization of the thermal motion as a useful resource. For instance, considering an ensemble of Λ-type three-level hot atoms, when the probe beam and coupling beam co-propagate in the atoms, the electromagnetically-induced-transparency (EIT) effect forms (the two-photon resonance can be satisfied because of the Doppler-free) [23]. However, if the probe beam counter-propagates with the coupling beam, strong absorption of the hot atoms prohibits the transmission of the probe beam due to the Doppler shift. This chiral response of atoms dependent on unidirectional coupling field breaks the system's time-reversal symmetry and enables ONR transmission of the probe light [18]. Furthermore, when combining this ensemble with an optical cavity, the enhancement of atomic nonlinearity can boost ONR's efficiency and sensitivity [21,22], which has facilitated the development of quantum devices, such as optical isolator [24,25], optical switching and routing [26–30], and all-optical logic gates [31–33].

In this paper, we experimentally demonstrated a scheme for performing ONR with a degenerate two-level atom-cavity system. For the degenerate transition F_g↔F_e with the ground-state angular momentum F_g is larger than the excited-state angular momentum F_e, we firstly study the transmission of the probe beam in free space. It is found that the ONR based on free-space EIT is not perfect due

 doi:10.20944/preprints202406.1244.v1

to the frequency degeneracy. Embedding the thermal degenerate atoms in a ring cavity, however, the cavity transmission can achieve ONR at the lower probe intensity, which benefits from the strong coupling property of the atom-cavity system. Qualitatively, combing all Zeeman sublevels of the atoms and the strong-coupling characteristics of the atom-cavity, we explained the experimental results. Finally, by changing the parameters of the coupling field, the ONR with high contrast and wide frequency-tuning range were experimentally investigated.

2. Experimental Arrangement and Results

The schematic diagram of our experimental setup is shown in Figure 1a. Two independent extended cavity diode lasers (ECDLs) with wavelength 894.5 nm are used as probe and coupling laser, respectively. In our experimental setup, we define the direction in which light travels from left to right as forward and the opposite direction as backward. The probe laser is divided into three parts by two combination of half-wave plate ($\lambda/2$) and polarization beam splitter (PBS): The first part is used for saturation absorption spectrum (SAS) and is detected by a photo detector (PD1); The second part is as the probe light of free-space EIT system and is detected by PD2; The third is also split into two parts (denoted by p_f and p_b) by a 50/50 beam-splitter (BS). A three-mirror ring cavity consists of two plane mirror C1 and C2 with the same transmissivity of 3%, and a plano-concave super mirror C3 with radius of curvature of 1000 mm and reflectivity of 99.99%, mounted on a piezoelectric transducer (PZT) for cavity frequency scanning and locking. The single cavity length L is about 530 mm. A 75-mm-long intracavity Cs cell with anti-reflection coated end windows is wrapped with μ-metal sheets for magnetic field shielding and wrapped in a heat tape for temperature-controlling. The weaker probe light p_f (p_b) with horizontal polarization reflected by transmissivity 90% beam-splitter (TS) is injected into C1 (C2) along the forward (backward) direction, and circulates in the atomic-cavity system as the cavity mode, then its output is detected by PD3 (PD4). The coupling laser is split into two parts (denoted by c_f and c_b) by a BS. The stronger coupling light c_f (c_b) with vertical polarization reflected by PBS passes through the Cs cell along the forward (backward) direction. Notably, the two counter-propagating coupling beams form a SW in the intracavity Cs cell and then are reflected out by two PBSs in void of circulation in the cavity. At the center of the cavity, the effective diameters of the probe and coupling lights are about 380 μm and 575 μm, respectively. The finesse of the ring cavity is degraded from 100 to 36 because of the linear loss of the inserted Cs cell and the two PBSs. The temperature of the Cs cell both in the free space and in the cavity is controlled at 40ºC.

The energy level diagrams of the atoms are shown in Figure 1b. Our experiment is performed in the D1 line of the ^{133}Cs atoms. The probe and coupling lasers drive the same transition $|6^2S_{1/2}, F_g=4\rangle \leftrightarrow |6^2P_{1/2}, F_e=3\rangle$. The coupling laser is frequency-locked to the nearby of transition frequency ω_{ge} with detuning Δ_c ($\Delta_c=\omega_c-\omega_{ge}$), and the probe laser is frequency-scanned across ω_{ge} with detuning Δ_p ($\Delta_p=\omega_p-\omega_{ge}$). Figure 1c,d show the interaction process of atom-cavity system when only p_f or only p_b injects the intracavity Cs vapor, respectively. We define $\Delta_q=\omega_q-\omega_{ge}$ as the detuning of the qth probe cavity mode from the atomic resonance frequency.

 doi:10.20944/preprints202406.1244.v1

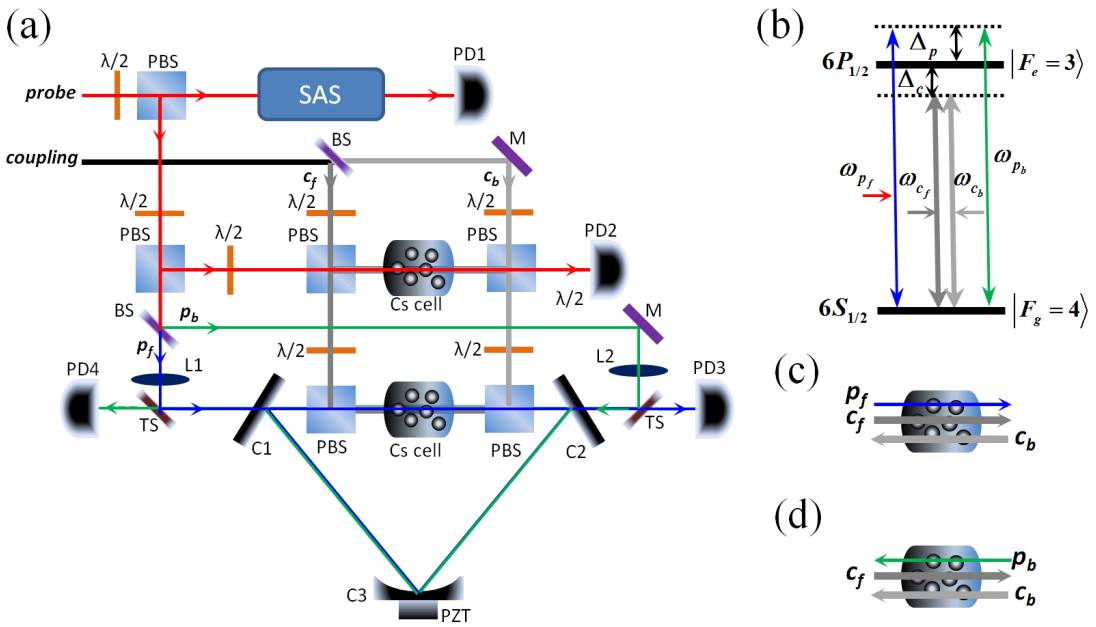

Figure 1. (**a**) Schematic of experimental setup. (**b**) Diagram of energy levels for the atoms. Two types for only p_f (**c**) or only p_b (**d**) is seeded into the atom-cavity system.

Figure 2 compares the transmission spectra of the probe light under the condition of different coupling field in free space, which is detected by PD2 in Figure 1a. The gray curve is the SAS of the probe laser, which is used to calibrate the transition level of the atom and judge the frequency detuning of the coupled laser. When only the co-propagating coupling field c_f is injected the Cs cell, a narrow transparency peak with linewidth ~1.2 MHz is obtained because the two photon resonance can be satisfied (that is Doppler free, $\Delta_p = \Delta_c$), i.e. the so-called EIT effect [23], as shown black curve (1) in Figure 2. Predictably, when only the counter-propagating c_b is injected, the EIT peak disappears due to the Doppler shift of the hot atom, as shown red curve (2) in Figure 2. However, a transparency with linewidth-broaden appears near the center of the two-photon resonance. This is because the frequency of the coupling light is the same as that of the probe light, and the stronger Rabi frequency of the coupling light occupies more the same ground state population of the atom. Thus the absorption of the atom to probe light is weakened. Notably, this is independent of the propagating direction of the coupling light. Therefore, there is still a weak probe light that can pass through the Cs cell, which leads to imperfect ONR. The standing-wave (SW) field c_s forms when c_f and c_b are simultaneously injected, which causes the periodic modulation on the refractive index of the atom, accompanied by anomalous dispersion and strong absorption of the probe light [34]. So a strong absorption pit appears at the center of two photon resonance, as shown blue curve (3) in Figure 2. That is so-called electromagnetically induce absorption effect (EIA) [35]. Here the probe light is forbidden to pass through the Cs cell whether it propagates along the forward or backward direction.

 doi:10.20944/preprints202406.1244.v1

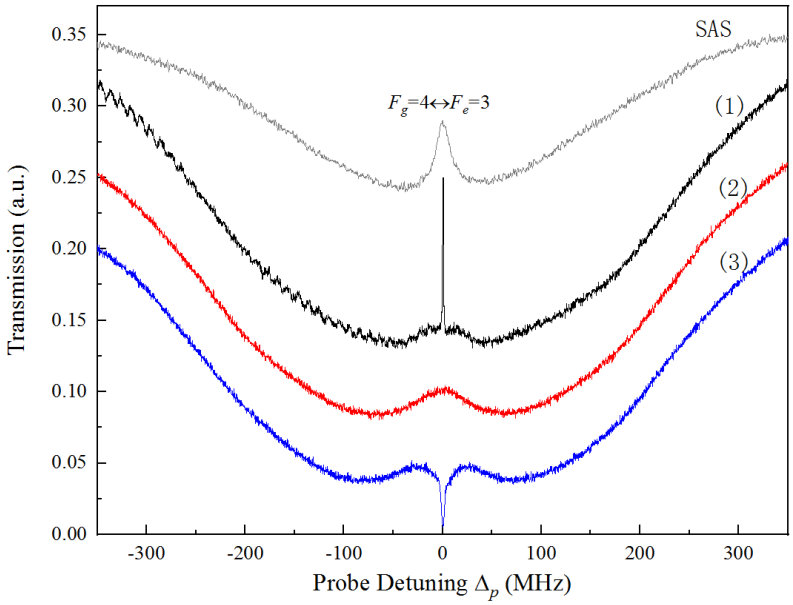

Figure 2. Transmission spectra of the probe light under different configurations of the coupling fields in free space: (1) only c_f with power $P_{c_f} = 1\,\mathrm{mW}$, (2) only c_b with $P_{c_b} = 1\,\mathrm{mW}$, and (3) SW c_s with $P_{c_f} = P_{c_b} = P_{c_s} = 1\,\mathrm{mW}$. The other experimental parameters are: $P_p = 10\ \mu\mathrm{W}$, $\Delta_c = 0$.

Inspired by the generation of ONR of three-level atom-cavity systems [18,22], we place degenerate two-level atoms in a three-mirror ring cavity (see Figure 1). Figure 3 plots the cavity transmission spectra of probe light at Δ_q=Δ_c=0. In the case of forward p_f [Figure 1c], when only forward c_f is injected ($P_{c_f} = 20\,\mathrm{mW}$), apart from two vacuum Rabi splitting (VRS) peaks which are resulted from the strong-coupling of the atom-cavity [36], a narrowed single dark-state peak (intracavity EIT) is observed at the atomic resonance center (Δ_p=0), as shown black line (1) in Figure 3a. Comparing to the EIT of free space, the linewidth of the single dark-state peak is narrowed to two times (~0.6 MHz), as shown embedded in Figure 3a. When only backward c_b is injected with $P_{c_b} = 20\,\mathrm{mW}$, a wide cavity mode without vacuum-Rabi-splitting appears at the atomic resonance center, as shown red line (2) in Figure 3a. When only the backward p_b is injected [Figure 1d], the results are just the opposite, as shown lines (1) and (2) in Figure 3b. Under the action of SW coupling field ($P_{c_s} = 20\,\mathrm{mW}$), however, regardless of p_f or p_b, the cavity transmission spectrum is similar: the central single-dark-state peak disappears because of EIA, meanwhile, the symmetrical double-dark peaks appear on either side of the atomic resonance center, as shown blue lines (3) in Figure 3a,b. It is worth emphasizing that although for p_f and p_b, their double dark-state peaks exhibit optical reciprocity (OR) due to the symmetry of the system, the transmission efficiencies are much lower than that of the single dark-state peak because the frequency position of the double dark-state peaks is not resonant with the cavity mode ($\Delta_q = 0$).

 doi:10.20944/preprints202406.1244.v1

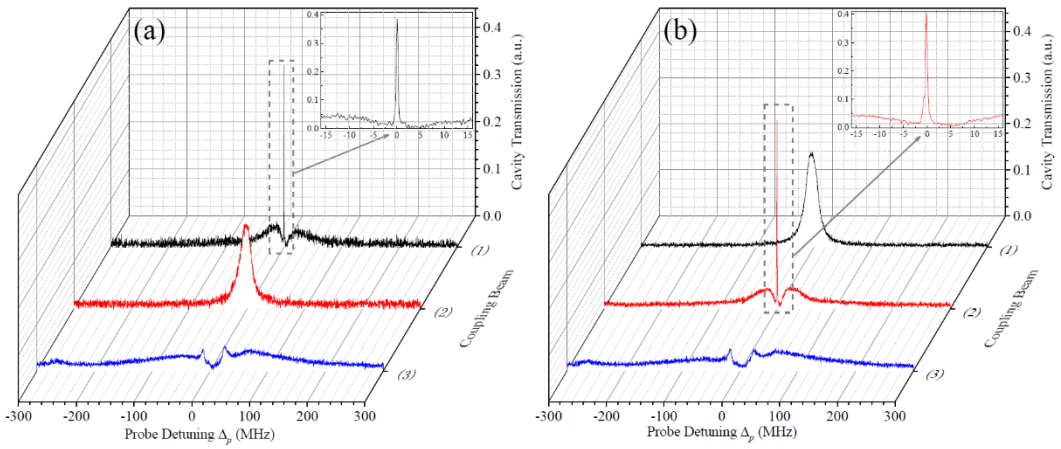

Figure 3. Cavity transmission spectra of the forward probe light p_f (a) and backward p_b (b) under three different coupling light conditions: (1) only c_f with $P_{c_f} = 20\ \mathrm{mW}$, (2) only c_b with $P_{c_b} = 20\ \mathrm{mW}$, and (3) c_s with $P_{c_s} = 20\ \mathrm{mW}$. The other experimental parameters are $P_{p_f} = P_{p_b} = 1.8\ \mathrm{mW}$ $T = 40^\circ\mathrm{C}$, and $\Delta_q = \Delta_c = 0$.

From Figure 3 we can see, when the probe light counter-propagates with the single coupling light, the cavity transmission show imperfect ONR (or OR) at the atom resonance center, which is different from that of the Λ-type three level atom-cavity system [18]. The reason is because in our experiment, the counter-propagating coupled light occupies part of the degenerate ground state atomic population, which reduces the absorption of intracavity atoms to the probe cavity mode and inhibits the strong-coupling efficiency of the atom-cavity system. When decreasing the input power of the probe light, the strong-coupling effect of the atom-cavity can be shown. Figure 4 shows the cavity transmission at $P_{p_f} = P_{p_b} = 0.4\ \mathrm{mW}$. When only co-propagating $p_{f(b)}$ and $c_{f(b)}$ are injected, a linewidth-narrowed intracavity EIT peak can be obtained at Δ_p=Δ_c=0, as shown in black line (1) in Figure4a or red line (2) in Figure 4b. When only counter-propagating $p_{f(b)}$ and $c_{b(f)}$ are injected, the cavity mode at atom resonance center disappears due to VRS effect, as shown in red line (2) in Figure 4a or black line (1) in Figure 4b. So the ONR of the probe cavity mode based on intracavity EIT is realized. Here, we define the contrast of ONR as $\eta = (T_{co} - T_{coun}) / (T_{co} + T_{coun})$ [14], where $T_{co(count)}$ is the intensity of the cavity transmission of the probe light co(counter)-propagates with the coupling field at Δ_p=Δ_c=0,. Whether it is p_f or p_b, the contrast η reaches nearly 90% (see embedded in Figure 4). Notably, at low probe power, due to the large absorption and linear loss of the atom-cavity system, both VRS peaks are very weak to almost invisible, which improves the contrast of ONR. In addition, the double dark-state peaks generated by the SW coupling field are also lost to be completely invisible, as shown in blue lines (3) in Figure 4.

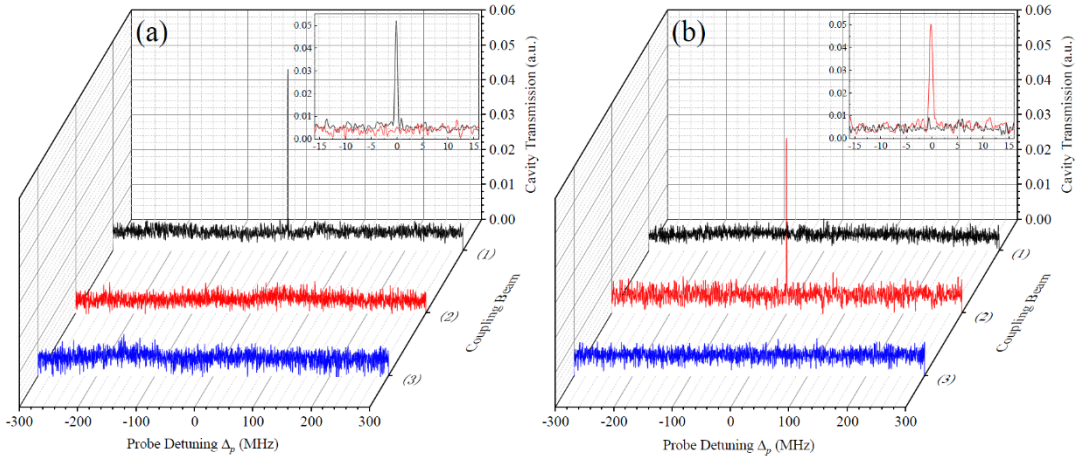

 doi:10.20944/preprints202406.1244.v1

Figure 4. Cavity transmission spectra of the forward probe light p_f (**a**) and backward p_b (**b**) with power $P_{p_f} = P_{p_b} = 0.4\ \mathrm{mW}$. The other experimental parameters are the same as those in Figure 3.

3. Theoretical Analysis and Further Experimental Investigation

Here, taking into account all Zeeman sublevels of the degenerate transition $F_g = 4 \leftrightarrow F_e = 3$, we provide a qualitative explanation of the experimental results. As is known, a linearly polarized beam consists of left-handed (σ^+) and right-handed (σ^-) circularly polarized components, which couple the corresponding σ transition. In our experiment, the coupling and probe beams are both linearly polarized and perpendicular to each other. For the co-propagating coupling and probe lights, the interaction between the σ^+ component of the coupling light and the σ^- component of the probe light (and vice versa) establishes (Doppler free), which leads to the formation of coherent population trapping (CPT) of all the Zeeman sublevels of the ground state and two stable Λ-type EIT chains [37], as shown in Figure 5. Therefore, the transmission of probe light in free space is transparency under the two-photon resonant condition (see Figure 2), which is the superposition of two Λ-type sublevel's action. Furthermore, with the help of the resonance filtering characteristics of the cavity, the intracavity EIT peak with linewidth-narrowed can also be obtained (see Figures 3 and 4).

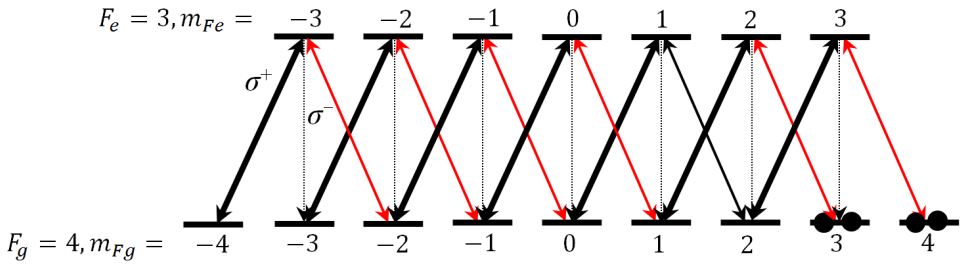

Figure 5. Zeeman sublevels for the degenerate transitions $F_g = 4 \leftrightarrow F_e = 3$.

Based on above consideration, the degenerate two-level transition $F_g = 4 \leftrightarrow F_e = 3$ can be simplified as a three-level system. Therefore, using the susceptibility theory of dicromatic coupling field acting on three-level atoms, the physical mechanism of single-double dark-state peak formation in two-level atom-cavity system can be well explained, and the detailed see Refs. [22,34]. As for the ONR based on intracavity EIT, however, the strong coupling effect of the degenerate two atom-cavity systems is different. The provision of a rigorous theoretical calculation is highly complex due to the necessity of accounting for all Zeeman sublevels. As such, here solely presents a qualitative analysis.

For the three-level atom-cavity, the coupling strength (the frequency space of VRS) is expressed as $\sqrt{g^2 N + 4^{-1}\Omega_c^2}$ [36,38], where g is the single photon coupling rate for the probe light, N is the number of involved intracavity atoms, and Ω_c is the Rabi frequency of the control field. So at the same Temperature (N) and coupling power (Ω_c), the strong coupling between the probe cavity mode and intracavity atoms induces a large VRS, which strongly suppresses the transmission of the probe light counter-propagating with the control field. This is more likely to induce the generation of ONR via EIT [18]. Differently, for the degenerate two-level atom-cavity, since the coupled light and probe light act on the same ground state, and $\Omega_c \gg \Omega_p$, the coupled light pumps more the same ground state atoms and reduces the effective atom number N. Although the coupling light also plays a role in improving the coupling intensity, there is competition behavior here. Clearly, weakening the coupling strength played a dominant role in our experiment. Therefore, on the basis of the presence of intracavity EIT, changing the probe optical power is an effective means to achieve ONR.

Experimentally, taking forward p_f for example, Figure 6 compares the variation of the cavity transmission intensity as a function of the probe power under different coupled light conditions.

 doi:10.20944/preprints202406.1244.v1

When only co-propagating c_f is injected, the intensity of single dark-state peak increases almost linearly with the probe power. Moreover, the stronger the coupling power, the steeper the slope of intensity growth. Here, the slope is defined as the ratio of the difference in cavity transmission intensity to the difference in input probe power. Such as, the growth slope of single dark-state peak increases from 0.11 to 0.22 when the power of c_f increases from 10 mW to 20 mW, as shown in solid and hollow squares in Figure 6a. For the case of only counter-propagating c_b, when $P_p \le 0.8$ mW, there is no probe cavity mode transmission due to the strong-coupling. That is, the ONR based on intracavity EIT is satisfied in this range, as shown the gray are in Figure 6b. Until $P_p > 0.8$ mW, the cavity transmission without VRS which destroy the ONR occurs, and increases lineally with the probe power, as shown in the circles in Figure 6b. As for the case of SW coupling field, due to the lower transmission efficiency and larger intracavity loss, the double dark-state peaks cannot appear until the probe power $P_p > 1.2$ mW, as shown in blue triangles in Figure 6c. The embedded in Figure 6a,c show the intensity of two VRS peaks under the condition of single co-propagating and SW coupling fields, respectively. Similar results can also be obtained for backward p_b and not repeated here.

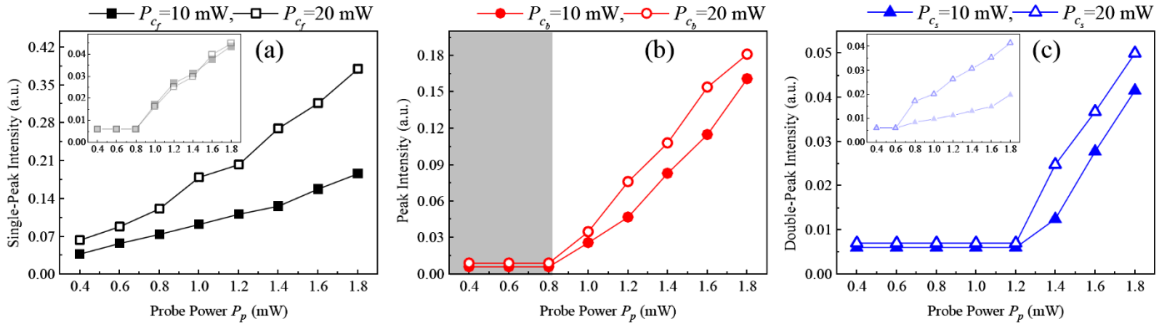

Figure 6. The cavity transmission intensity of p_f versus the input probe power. The other experimental parameters are the same as in Figure 3.

Furthermore, the impact of frequency detuning of the coupling field on ONR has also been experimentally investigated. Based on Figure 2a, Figure 7 presents the cavity transmission of p_f under the different coupling detuning Δ_c. For the case of only co-propagating c_f, the intracavity EIT peak shifts with Δ_c, as shown in Figure 7a. Notably the cavity mode detuning Δ_q hardly changes the frequency point, but it affects the intensity of intracavity EIT. The optimal transmission output occurs at Δ_c=Δ_c. For the case of only counter-propagating c_b, there is no transmission (including VRS) detected, as shown in Figure 7b. Experimentally, the ONR transmission with high contrast (up to 90%) and narrowed linewidth (about 0.6 MHz) can be obtained in the range of Δ_c=±150 MHz. Actually, there is still intracavity EIT signal at larger coupling detuning, but the transparency efficiency is very weak due to far-off atomic resonance, which should reduce the contrast of ONR.

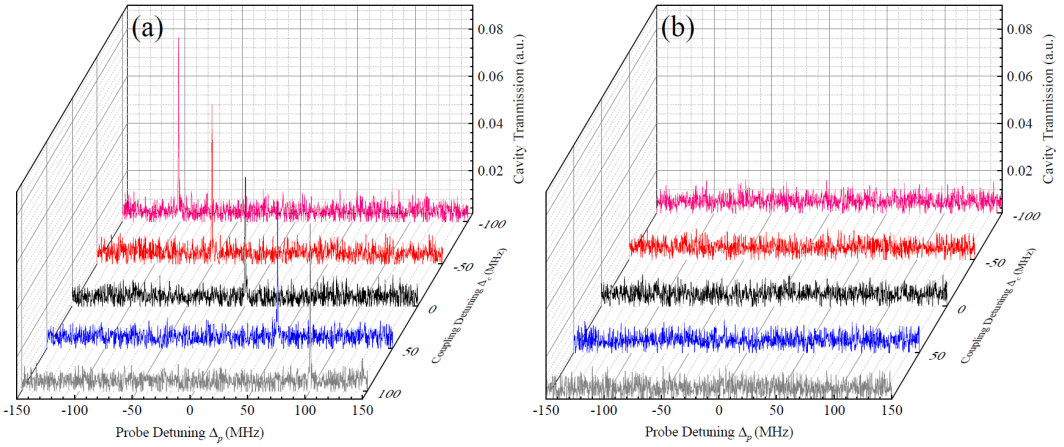

 doi:10.20944/preprints202406.1244.v1

Figure 7. Cavity transmission spectra of p_f under various coupling detuning. (**a**) only c_f, and (**b**) only c_b. The other experimental parameters are the same as those in Figure 3.

It is worth emphasizing that the temperature of intracavity Cs cell is also a factor affecting the cavity transmission. In our experiment, there is a good ONR transmission within the range of 35ºC～50 ºC. Certainly, the other parameters range which confirm to ONR should vary slightly.

4. Conclusions

In conclusion, using degenerate two-level atom-cavity combined system, we have experimentally implemented ONR based on intracavity EIT. For the degenerate transition $F_g \leftrightarrow F_e$ ($F_g > F_e$), the linewidth-narrowed single dark-state peak generates when the probe cavity mode co-propagates with the coupling field (Doppler free), which results from the stable Λ-type coherence chains of all the Zeeman sublevels of the ground state. This is similar to the result for three-level atom-cavity system. But differently, when the two beams counter-propagate, the larger Rabi frequency of the coupling field can consume more of the population of the same ground state due to the frequency degeneracy, which reduces the number of effective atoms acted on the cavity mode and weakens the strong-coupling strength of the atom-cavity. Therefore, the ONR based on intracavity EIT can only be satisfied at very weak probe intensity. The study further enriches the physical extension of ONR and also can be applied in quantum information processing. Furthermore, due to the same frequency of the lights, only one laser is needed to implement our experimental scheme, which should indeed be highly useful in the design of integrated optical quantum devices, such as optical switching and routing, logical gate manipulation.

Author Contributions: Conceptualization, C.-Z.Q. and H.-T.Z.; methodology, C.-Z.Q. and D.W.; software, R.-N.L.; validation, J.-R.Z. and Y.-H.T.; formal analysis, C.-Z.Q. and L.-H.H.; investigation, C.-Z.Q. and H.-T.Z.; resources, H.-T.Z. and L.-H.H.; data curation, C.-Z.Q.; writing—original draft preparation, C.-Z.Q.; writing—review and editing, H.-T.Z. All authors have read and agreed to the published version of the manuscript.

Funding: This work was supported by National Natural Science Foundation of China (Grant Nos. 61975102, and 11704235); Natural Science Foundation of Shanxi Province, China (Grant No. 20210302123437), and the Fund for Shanxi Key Subjects Construction.

Data Availability Statement: Data are contained within the article.

Conflicts of Interest: The authors declare no conflicts of interest.

References

1. Estep, N.D.; Sounas, J.; Soric, A.; Alù, A. Magnetic-free non-reciprocity and isolation based on parametrically modulated coupled-resonator loops. *Nature Phys.* **2014**, *10*, 923–927.
2. Lodahl, P.; Mahmoodian, S.; Stobbe, S.; Rauschenbeutel, A.; Schneeweiss, P.; Volz, J.; Pichler, H.; Zoller, P. Chiral quantum optics. *Nature* **2017**, *541*, 473–480.
3. Jalas, D.; Petrov, A.; Eich, M.; Freude, W.; Fan, S.; Yu, Z.; Baets, R.; Popović, M.; Melloni, A.; Joannopoulos, J.D.; Vanwolleghem, M.; Doerr, C.R.; Renner, H. What is — and what is not — an optical isolator. *Nature Photon.* **2013**, *7*, 579–582.
4. Aplet, L.J.; Carson, J.W. A Faraday effect optical isolator. *Appl. Opt.* **1964**, *3*, 544–545.
5. Peng, B.; Özdemir, S.K.; Lei, F.; Monifi, F.; Gianfreda, M.; Long, G.L.; Fan, S.; Nori, F.; Bender, C.M.; Yang, L. Parity-time-symmetric whispering-gallery microcavities. *Nat. Phys.* **2014**, *10*, 394–398.
6. Ganainy, R.E.; Makris, K.G.; Khajavikhan, M.; Musslimani, Z.H.; Rotter, S.; Christodoulides, D.N. Non-Hermitian physics and PT symmetry. *Nat. Phys.* **2018,** *14*, 11–19.
7. Buddhiraju, S.; Song, A.; Papadakis, G.T.; Fan, S.H. Nonreciprocal metamaterial obeying time-reversal symmetry. *Phys. Rev. Lett.* **2020**, *124*, 257403.
8. Xu, W.; Iyer, A.; Jin, L.; Set, S.Y.; Renninger, W.H. Strong optomechanical interactions with long-lived fundamental acoustic waves. *Optica* **2023**, *10*, 206-213.
9. Xu, H.; Jiang, L.Y.; Clerk, A.A. Harris, J.G.E. Nonreciprocal control and cooling of phonon modes in an optomechanical system. *Nature* **2019**, *568*, 65–69.
10. Lépinay, L.M.; Ockeloen-Korppi, C.F.; Malz, D.; Sillanpää, M.A. Nonreciprocal transport based on cavity floquet modes in optomechanics. *Phys. Rev. Lett.* **2020**, *125*, 023603.

 doi:10.20944/preprints202406.1244.v1

11. Scheucher, M.; Hilico, A.; Will, E.; Volz, J.; Rauschenbeutel, A. Quantum optical circulator controlled by a single chirally coupled atom. *Science* **2016**, *354*, 1577–1580.
12. Söllner, I.; Mahmoodian, S.; Hansen, S.L.; Midolo, L.; Javadi, A.; Kiršanské, G.; Pregnolato, T.; El-Ella, H.; Lee, E.H.; Song, J.D.; Stobbe, S.; Lodahl, P. Deterministic photon–emitter coupling in chiral photonic circuits. *Nat. Nanotechnol.* **2015**, *10*, 775–778.
13. Hua, S.; Wen, J.; Jiang, X.; Hua, Q.; Jiang, L.; Xiao, M. Demonstration of a chip-based optical isolator with parametric amplification. *Nat. Commun.* **2016**, *7*, 13657.
14. Wang, D.W.; Zhou, H.T.; Guo, M.J.; Zhang, J.X.; Evers, J.; Zhu, S.Y. Optical diode made from a 289 moving photonic crystal. *Phys. Rev. Lett.* **2013**, *110*, 093901.
15. Biancalana, F.; Amann, A.; Uskov, A.V.; O'Reilly, E.P. Dynamics of light propagation in spatiotemporal dielectric structures. *Phys. Rev. E* **2007**, *75*, 046607.
16. Horsley, S.A.R.; Wu, J.H.; Artoni, M.; La Rocca, G.C. Optical nonreciprocity of cold atom Bragg mirrors in motion. *Phys. Rev. Lett.* **2013**, *110*, 223602.
17. Yang, P.F.; Xia, X.W.; He, H.; Li, S.K.; Han, X.; Zhang, P.; Li, G.; Zhang, P.F.; Xu, J.P.; Yang, Y.P.; Zhang, T.C. Realization of nonlinear optical nonreciprocity on a few-photon level based on atoms strongly coupled to an asymmetric cavity. *Phys. Rev. Lett.* **2019**, *123*, 233604.
18. Zhang, S.; Hu, Y.; Lin, G.; Niu, Y.; Xia, K.; Gong, J.; Gong,S. Thermal-motion-induced non-reciprocal quantum optical system. *Nat. Photon.* **2018**, *12*, 744–748.
19. Lin, G.W.; Zhang, S.C.; Hu, Y.Q.; Niu,;Y.P.; Gong, J.B. Gong, S.Q. Nonreciprocal amplification with four-level hot atoms. *Phys. Rev. Lett.* **2019**, *123*, 033902.
20. Hu, H.Q.; Zhang, S.H.; Kuang, X.Y.; Qi, Y.H.; Lin, G.W.; Gong, S.Q.; Niu, Y.P.; Reconfigurable nonreciprocity with low insertion loss using a simple two-level system. *Opt. Express* **2020**, *28*, 38710–38717.
21. Liang, C.; Liu, B.; Xu, A.N.; Wen, X.; Lu, C.C.; Xia, K.Y.; Tey, M.K.; Liu, Y.C.; You, L. Collision-induced broadband optical nonreciprocity. *Phys. Rev. Lett*. **2020**, *125*, 123901.
22. Zhou, H.T.; Xie, S.Y.; Li, X.; Wang, D.; Yang, B.D.; and Zhang, J.X. Manipulation of optical nonreciprocity in hot atom-cavity system. *J. Phys. B: At. Mol. Opt. Phys.* **2021**, *54*, 195001.
23. Harris, S.E.; Field, J.E.; Imamoğlu, A. Nonlinear optical processes using electromagnetically induced transparency. *Phys. Rev. Lett*. **1990**, *64*, 1107–1110.
24. Khanikaev, A.B.; Alù, A. Nonlinear dynamic reciprocity. *Nat. Photon.* **2015**, *9*, 359–361.
25. Chen, W.T.; Liu, L.; Zhao, J.; Zhang, C. On-chip broadband, compact TM mode Mach–Zehnder optical isolator based on InP-on-Insulator platforms. *Nanomaterials* **2024**, *14*, 709.
26. Dawes, A.; Illing, L.; Clark, S.M.; Gauthier, D.J. All-optical switching in rubidium vapor. *Science* **2005**, *29*, 672–674.
27. Wang, C.Y.; Chen, Y.F.; Lin, S.C.; Lin, W.H.; Kuan, P.C.; Yu, I.A. Low-light-level all-optical switching. *Opt. Lett*. **2006**, *31*, 2350–2352.
28. Sheng, J.; Khadka, U.; Xiao, M. Realization of All-Optical Multistate Switching in an Atomic Coherent Medium. *Phys. Rev. Lett*. **2012**, *109*, 223906.
29. Chang, D.E.; Sørensen, A.S.; Demler, E.A.; Lukin, M.D. A single-photon transistor using nanoscale surface plasmons. *Nat. Phys*. **2007**, *3*, 807–812.
30. Saha, S.; Diroll, B. T.; Ozlu, M. G.; Chowdhury, S. N.; Peana, S.; Kudyshev, Z.; Schaller, R. D.; Jacob, Z.; Shalaev, V. M.; Kildishev, A. V. Engineering the temporal dynamics of all-optical switching with fast and slow materials. *Nat. Commun.* **2023**, *14*, 5877.
31. Mondal, H.; Goswami, K.; Sen, M.; Khan, W.R. Design and analysis of all-optical logic NOR gate based on linear optics. *Opt. Quant. Electron*. **2022**, *54*, 272.
32. de Clercq, L.E.; Lo, H.Y.; Marinelli, M.; Nadlinger, D.; Oswald, R.; Negnevitsky, V.; Kienzler, D.; Keitch, B.; Home, J.P. Parallel transport quantum logic gates with trapped ions. *Phys. Rev. Lett*. **2016**, *116*, 080502.
33. Babazadeh, A.; Erhard, M.; Wang, F.; Malik, M.; Nouroozi, R.; Krenn, M.; Zeilinger, A. High-dimensional single-photon quantum gates: Concepts and experiments. *Phys. Rev. Lett*. **2017**, *119*, 180510.
34. Zhang, J.X.; Zhou, H.T.; Wang, D.W.; Zhu, S.Y. Enhanced reflection via phase compensation from anomalous dispersion in atomic vapor. *Phys. Rev. A* **2011**, *83*, 053841.
35. Lezama, A.; Barreiro, S.; Akulshin, A.M. Electromagnetically induced absorption. *Phys. Rev. A* **1999**, *59*, 4732-4735.
36. Wu, H.B.; Gea-Banacloche, J.; Xiao, M. Observation of intracavity electromagnetically induced transparency and polariton resonances in a Doppler-broadened medium. *Phys. Rev. Lett*. **2008**, *100*, 173602.
37. Zhou, H.T.; Guo, M.J.; Wang, D.; Gao, J.R.; Zhang, J.X.; Zhu, S.Y. Angular momentum and two-photon detuning dependence of reflection spectrum on degenerate two-level systems in Cs vapour. *J. Phys. B: At. Mol. Opt. Phys*. **2011**, *44*, 225503.
38. Mücke, M.; Figueroa, E.; Bochmann, J.; Hahn, C.; Murr, K.; Villas-Boas C.J.; Rempe, G. Electromagnetically induced transparency with single atoms in a cavity. *Nature* **2010**, *465*, 755-758.

 doi:10.20944/preprints202406.1244.v1